Vol. 08, No. 2 (2026) 1231-1240, doi: 10.24874/PES08.02B.012

Proceedings on Engineering Sciences

www.pesjournal.net

DEVELOPMENT OF NANOMATERIAL BASED MICROFLUIDIC POINT OF CARE TESTING DEVICE

Manasi Mahajan
Manisha R.
Reena Monica P.[1]

Received 19.04.2025
Revised 12.06.2025
Accepted 17.07.2025

Keywords:

Microfluidics, Point of care devices, Organ on Chip, Polydimethylsiloxane, Extracellular Matrix, Sensitivity, Ansys Fluent, Microchannel, Versatility

A B S T R A C T

Microfluidics has emerged as a transformative field that manipulates small amounts of fluids to revolutionize diagnostics. Integrating microfluidic devices into point-of-care testing improves accuracy, speed and accessibility, ultimately improving patient care. These devices enable fast and accurate analysis through efficient mass transport mechanisms. Microfluidic devices typically consist of micro channels, micropumps and microreactors. Some common applications include point-of-care diagnostics, DNA analysis, drug delivery, chemical synthesis, and environmental monitoring. Organ-on-chip (OOC) technology comprises living cells arranged to mimic the mechanical and physiological characteristics of actual organs. Typically, OOC devices are built of small channels or chambers connected by microfluidics that are transparent, like silicone or glass. The complex web of blood arteries and tissues seen in actual organs is replicated in these channels. Applications for OOC (Organ-On-A-Chip) technology are numerous and span a number of industries, including toxicology, pharmaceutical development, biomedical research, and personalized medicine. The design of Organ on chip design is designed, modelled and analysed in Ansys Fluent software.

© 2026 Published by Faculty of Engineering

1. INTRODUCTION

Organ-on-chip (OOC) technology has developed as a progressive approach in biomedical designing, advertising an advanced stage to imitate the structure and work of human organs in vitro (Wu et al., 2016). The innovation holds a colossal guarantee for progressing drug revelation, illness modelling, and personalized pharmaceuticals (Cui & Wang, 2019). The research presents the design, modelling, and examination of an organ-on-chip gadget utilizing Ansys Fluent software combined with the field of microfluidics. The integration of microfluidics with OOC innovation empowers exact control over the stream of supplements, oxygen, and other biochemical signals to cells processed on the chip (Kamholz et al., 1999; Datta & Ghosal, 2009). Such controlled microenvironments are essential for mimicking in vivo physiological conditions and ensuring accurate experimental outcomes (Gervais et al., 2006). Central to the analysis is the utilization of Ansys Fluent, effective CFD (Computational Fluid Dynamics) software, for the

[1] Corresponding author: Reena Monica P.
e-mail: reenamonica@vit.ac.in

plan, modelling, and investigation of the microfluidic properties of the OOC device (Tan et al., 2004; Xu & Attinger, 2008). By leveraging Ansys Fluent, the focus is to re-enact and optimize the fluid stream designs inside the chip and guarantee effective supplement conveyance (Kirpo, 2013; Rybdylova et al., 2016). Moreover, the approach includes the importation of blood information into Ansys Fluent, permitting it to mimic the stream characteristics of blood inside the OOC gadget, enabling it to imitate the physiological conditions experienced by organs in vivo (Chakraborty, 2005). By combining experimental analysis with computational modelling, research lines create a comprehensive understanding of the fluid elements inside the OOC gadget, clearing the way for improved applications in medicate disclosure, infection modelling, and personalized pharmaceuticals (Park et al., 2011). The insights gained from this research pave the way for enhanced applications in drug discovery, allowing for more accurate testing of pharmaceuticals in a controlled, organ-like environment (Nie et al., 2007; Tiwari et al., 2020).

2. ORGAN-ON-CHIP

2.1 A Respiration Process

In human respiration, the exchange of oxygen and carbon dioxide between the blood and lungs is crucial. This process occurs in the alveoli, tiny air sacs in the lungs. When air is inhaled, it reaches the alveoli, which are surrounded by a network of capillaries. The walls of both the alveoli and the capillaries are extremely thin, allowing gases to pass through them easily. Oxygen from the air in the alveoli diffuses into the blood because of a concentration gradient: the oxygen concentration is higher in the alveoli than in the blood (Kamholz et al., 1999). Conversely, carbon dioxide, which is a waste product of cellular metabolism, is higher in concentration in the blood than in the alveoli. This gradient drives carbon dioxide to diffuse from the blood into the alveoli.

Haemoglobin, a protein in red blood cells, plays a critical role in this gas exchange. It has a high affinity for oxygen, which allows it to bind oxygen molecules efficiently as they diffuse into the blood. This forms oxyhemoglobin, which is then transported throughout the body to deliver oxygen to cells for metabolic processes. Simultaneously, haemoglobin also binds to carbon dioxide, forming carboxyhemoglobin. This is how carbon dioxide is transported back to the lungs. When the blood reaches the lungs, the carbon dioxide is released from the hemoglobin and diffuses into the alveoli (Datta & Ghosal, 2009). During expiration, this carbon dioxide is expelled from the body. This gas exchange process is essential for maintaining the body's pH balance and ensuring that tissues receive adequate oxygen for cellular respiration and energy production, while also removing carbon dioxide, a by-product of metabolism. Organ-on-chip (OOC) devices operate on the principle of replicating the physiological functions of human organs. Recent advances in microfluidic device design highlight the versatility of these systems for biomedical applications (Zhou et al., 2013)

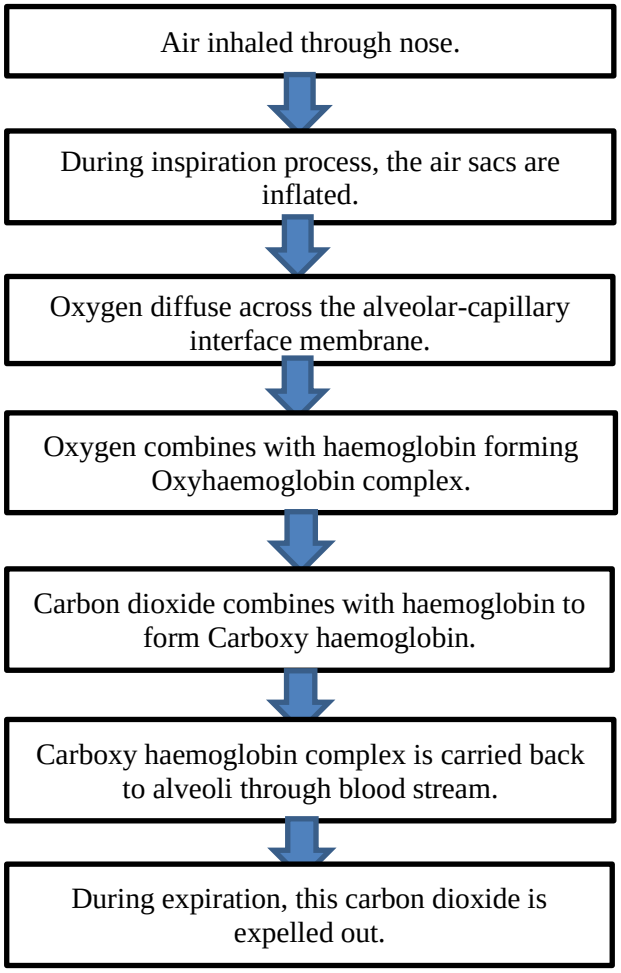


Figure 1. Human Respiratory System

As shown in Figure 1, the respiration process involves oxygen diffusing across the alveolar-capillary membrane, binding with haemoglobin to form oxyhemoglobin, while carbon dioxide forms carboxyhemoglobin and is carried back to the alveoli for expulsion.

Organ-on-chip (OOC) devices operate on the principle of replicating the physiological functions of human organs in a microfluidic platform. Usually made up of living cells lining micro-engineered tubes, these devices mimic the structure and functionality of certain organs like the liver, heart, or lungs. Previous work in tissue engineering and biomaterials has demonstrated the potential of microfluidic systems to replicate physiological environments (Khademhosseini et al., 2004). The working principle involves the precise manipulation of fluid flow, nutrient delivery, and waste removal within these microfluidic channels to recreate the in vivo tissue microenvironment. By incorporating

multiple cell types, including parenchymal cells, stromal cells, and vascular endothelial cells, OOC devices can replicate tissue- tissue interfaces and cellular interactions essential for organ function and disease modelling. The controlled microenvironment provided by the microfluidic channels enables researchers to study organ-level responses to stimuli, such as drugs or toxins, with higher physiological relevance compared to traditional cell culture systems. OOC technology allows for real-time monitoring of cellular behaviour, biochemical signalling, and tissue morphology, providing insights into organ physiology, disease mechanisms, and drug efficacy. Low-cost diagnostic platforms, such as paper-based microfluidics, have further expanded accessibility (Mertaniemi et al., 2012).Ultimately, the working principle of organ-on-chip devices facilitates the development of more accurate models for drug screening, toxicity testing, disease modelling, and personalized medicine, with the potential to revolutionize biomedical research and healthcare.

2.2 Design of organ on chip device

A significant perspective in making viable organ surrogates is the reliable generation of both, the ordinary tissue-tissue interfacing and the complex physiological microenvironment in which cells dwell. Lung-on-a-chip device is created which meticulously recreates the critical alveolar-capillary interface found in the lung air sac (Chow et al., 2005).
The lung-on-a-chip device consists of a 3D microfluidic platform comprising two parallel microchannels separated by a thin, porous, and flexible membrane made of poly(dimethylsiloxane) (PDMS) coated with extracellular matrix (ECM). These microchannels' dimensions—roughly 400 µm in width and 100 µm in height—approximately match the typical alveolar diameter found in human lungs. The hollow full-height chambers that encircle these microchannels are used to apply cyclic suction, which stretches and relaxes the flexible PDMS membrane inside the central channel mechanically. The physiological mechanism of breathing in living humans is the source of inspiration for the design. During inspiration, sub-atmospheric pressure is created in the lungs, which causes the alveolar air sacs to expand. This expansion causes the alveolar epithelium and adjacent vascular endothelium in capillaries to stretch.

The subsequent crucial phase is the seeding of pulmonary microvascular endothelial cells into the lower microchannel and human alveolar epithelial cells into the upper microchannel. These cells are allowed to grow into closely spaced tissue monolayers that resemble the alveolar-capillary interface by being cultured on the ECM-coated membrane for a minimum of five days. Continuous perfusion of culture medium through both channels ensures the provision of nutrients to the cells and the removal of metabolic wastes. The culture medium in the upper channel is replaced with air at confluence, resulting in the formation of an air-liquid interface at the alveolar epithelium's apical surface. The transition induces cellular differentiation and expression of tissue-specific functions, like surfactant production, akin to physiological conditions in the lung. Maintaining medium flow in the lower channel, meanwhile, provides oxygen and nutrients to the epithelium via the intervening endothelium, simulating the dynamic perfusion seen in pulmonary capillary blood vessels.

The elastic vertical walls of the center microchannel flex outward when a vacuum is given to the side hollow chambers, simulating lung breathing motions. The PDMS membrane and the associated epithelial and endothelial monolayers are stretched laterally by this mechanical deformation. After the “vacuum is released, the flexible feature of PDMS allows the layer to revert to its original length, unravelling the tissue layers. Through the recurrence of this actuation cycle at a frequency of 0.25 Hz and the regulation of the stretching level to yield roughly 10% cyclic” strain, the apparatus can induce dynamic mechanical distortions that are comparable to those found in the air sacs of a living human lung (Gervais et al., 2006).

Table 1. Database of Blood properties

Property	Count
Density	1.06 g/mL
Viscosity	3.5 cP at 310.15 K
Volume	4.5 liters
Temperature	310.15 K

3. DESIGN AND ANALYSIS ON ANSYS FLUENT

ANSYS Fluent is a CFD software package developed by ANSYS Inc., designed for simulating fluid flow and heat transfer phenomena (Gao et al., 2012; Kirpo, 2013). Geometric models can be designed, imported, and simulated. It involves creating complex 3D shapes, surfaces, and volumes. Figure 2 shows the design and modelling of the lung of the chip device.

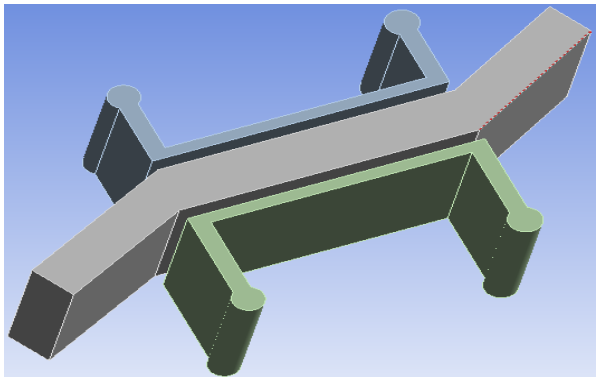


Figure 2. Design and modelling of lung on chip device on Ansys fluent software

In the initial design of the microfluidic lung-on-chip device, the inlets and outlets are curved. This curved design presents a challenge: when selecting one edge for an inlet or outlet, the selection process tends to include the entire surface due to the curvature. This issue complicates the precise control needed for microfluidic applications.

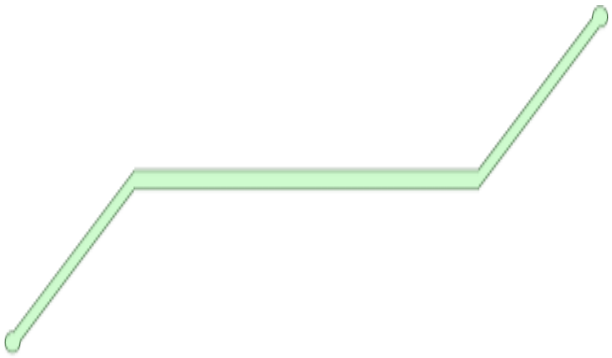


Figure 3. Upper Channel of the design

To address this problem, both the inlet and outlet edges are modified. Instead of maintaining their curved shapes as shown in Figure 3, these edges are sliced into a rectangular form. This adjustment simplifies the selection process, allowing for precise and distinct identification of the inlet and outlet edges. By converting the curved edges into rectangular shapes, we ensure that only the intended edge is selected, enhancing the accuracy and functionality of the microfluidic device. This modification is crucial for maintaining the integrity of fluid flow and ensuring the device operates as designed.

A detailed visualization of the microfluidic lung-on-chip geometry is provided in Figure 4, which shows a zoomed view of the design. This close-up highlights the structural features of the channels and membranes that are critical for accurate meshing and simulation. Alternative approaches, including acoustic wave-based microfluidics, have also been explored for precise fluid manipulation (Yaralioglu et al., 2004).Meshing used for precise fluid manipulation, is the process of dividing the geometric model into small elements to solve fluid flow equations numerically. ANSYS Fluent provides several meshing techniques structured, unstructured, and hybrid meshing to accurately represent the geometry. When mesh count or density is not specified explicitly in ANSYS Fluent, the software generates what is known as the default mesh. Figure 5 shows the default mesh.
Figure 6 shows the mesh XY plot of the design. In structured meshing, the computational domain is divided into a grid of regularly shaped elements, such as rectangles in 2D or hexahedra in 3D, aligned with the coordinate axes. Figure 7 shows the structured mesh, the element size is set to 0.000001 micrometres.

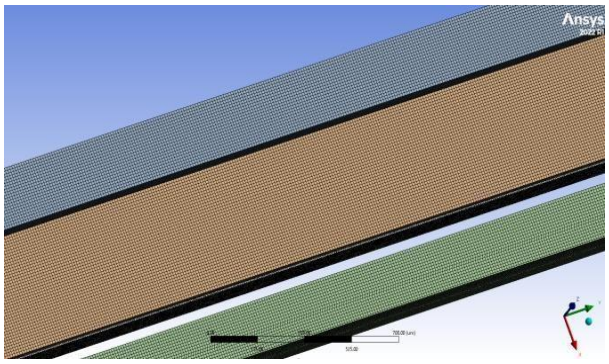


Figure 4. Zoomed view of the design

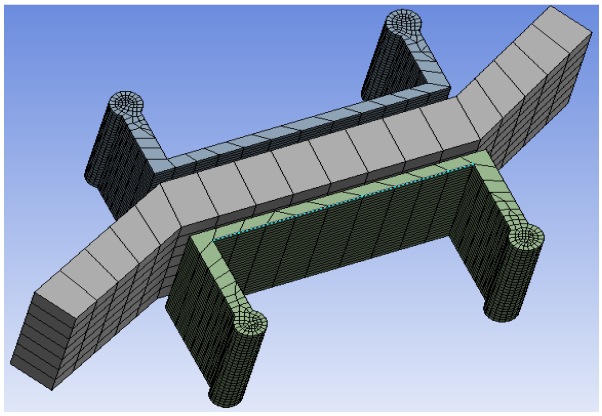


Figure 5. Default mesh of the design

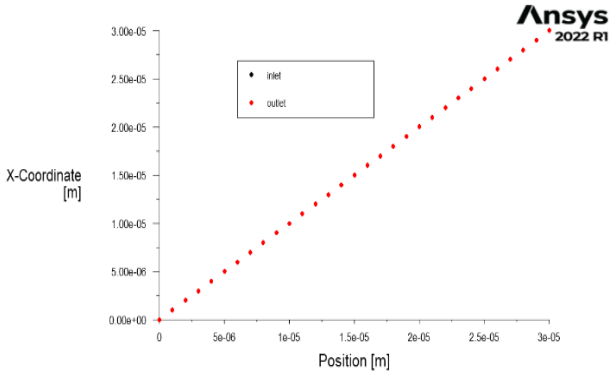


Figure 6. Mesh XY plot of the design.

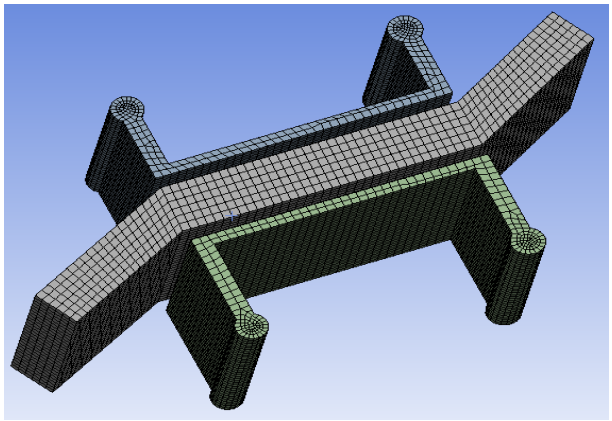


Figure 7. Structured mesh of the design.

The ratio of a cell's longest edge length to its shortest edge length in the mesh is known as the aspect ratio. A high aspect ratio indicates that the element is highly elongated or distorted, while a low aspect ratio indicates that the element is more regular in shape. The aspect ratio values range from a minimum of 1.0271 to a maximum of 7.1739, with a median value falling between 3.076 and 3.759. The maximum aspect ratio of 7.1739 indicates that some elements in the mesh are highly elongated or distorted. The minimum aspect ratio of 1.0271 suggests that there are elements in the mesh that are nearly equilateral or close to being regular in shape. Cyclic suction chambers tend to have median aspect ratio values whereas the rest of the design has a minimum aspect ratio. Figure 8 shows the aspect ratio of the design.

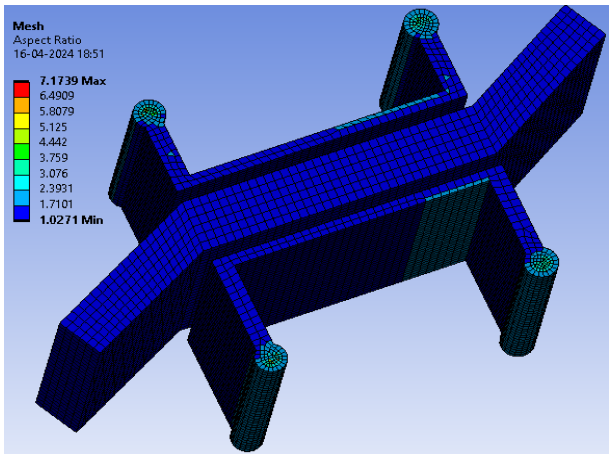


Figure 8. Aspect ratio of the design

Skewness is a measure of the quality of the mesh elements, It indicates how close the shape of each element is to an ideal shape. A maximum value of 0.57045 is relatively high, suggesting that some elements may be significantly distorted. The minimum value of 1.3058e-10 is extremely close to zero, indicating very high-quality mesh elements. The median value ranges from 0.25353 to 0.31692, indicating that a significant portion of the mesh elements have skewness values within this range. The inlets, outlets, and cyclic suction chambers have medium skewness values, suggesting that these regions may have slightly less optimal mesh quality compared to the rest of the design. Skewness, as shown in Figure 9, which illustrates the distribution of skewness values across the computational domain. The results indicate that while most elements exhibit low skewness (close to ideal), certain regions such as the inlets and cyclic suction chambers show moderately higher values, reflecting slight geometric distortions..

The setup function prepares the computational domain for the simulation after meshing. The stage involves defining boundary conditions, material properties, solver settings, and other parameters necessary for solving the fluid flow or other physical phenomena within the domain. One of the primary tasks in the setup function is defining boundary conditions. It entails describing the fluid's interactions with the computational domain's boundaries. Boundary conditions can include inlet conditions such as velocity, outlet conditions, wall conditions like no-slip or specified shear stress, symmetry conditions, and periodic conditions.

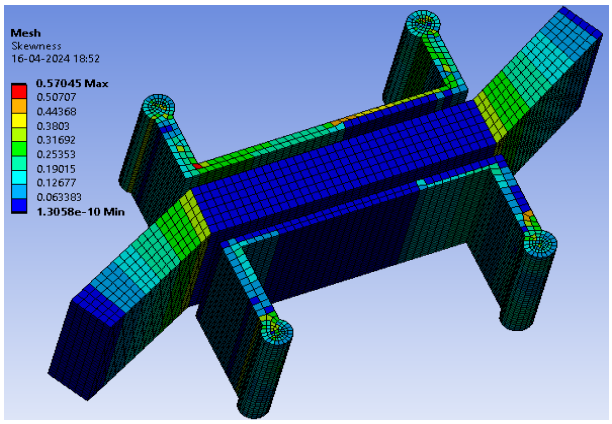


Figure 9. Skewness of the design

The properties of the fluid or fluids being simulated need to be defined accurately. This includes parameters such as density, viscosity, volume, and temperature. Table 1 shows the information on property and the respective count with units specified as per Ansys fluent software. When the blood database is imported for simulation, various parameters are specified in the material properties section (Chakraborty, 2005). Density represents the mass per unit volume of the fluid. The density of blood is specified as 1.06 grams per millilitre (g/mL) and influences the pressure distribution and fluid flow patterns within the system. The resistance of a fluid to flow is measured by its viscosity. Blood viscosity is specified as 3.5 centipoise (cP) which affects the rate of flow and shear stress distribution within the fluid domain. The volume parameter specifies the total volume of the blood within the computational domain which is specified as 4.5 litres. The volume parameter is relevant for defining the initial conditions and boundary conditions of the simulation. Temperature represents the thermal energy of the fluid. Blood temperature is specified as 310.15 Kelvin (K), which is approximately equal to 37 degrees Celsius. Temperature influences the viscosity and density of the blood, affecting its flow characteristics.

Before starting the actual simulation, the initial conditions of the flow field need to be specified. This involves assigning initial values of velocity, pressure, temperature, and any other relevant flow variables throughout the domain. Proper initialization helps in achieving a stable and convergent solution faster during the iterative solution process. The solver performs a specified number of iterations to advance the solution towards convergence. The iteration count is set to 1000, meaning that the solver will iterate

through the solution process 1000 times. Each iteration involves updating the flow field based on the current solution, applying boundary conditions, and evaluating convergence criteria.

When visualizing results in Fluent, contours are graphical representations that depict the distribution of various properties within the simulated domain. Velocity contour is a post-processing tool used to visualize the velocity distribution in a fluid flow simulation conducted using ANSYS Fluent. The contour plot displays the velocity field across the entire computational domain or specific sections of interest. This spatial representation allows users to observe how velocity varies across different regions, such as near boundaries, in flow stagnation zones, or within turbulent flow regions. They illustrate the influence of boundary conditions on fluid flow. For instance, near walls or solid objects, velocity gradients may be steep due to boundary layer effects or flow separation. By examining velocity contours, engineers can evaluate the impact of boundary conditions on flow behaviour and optimize designs accordingly. In transient simulations, velocity contours can be visualized at different time steps to observe how flow patterns evolve over time. This dynamic visualization is crucial for understanding unsteady flow behaviour, transient phenomena, and the effects of time-varying boundary conditions or fluid properties. Figure 10 shows the velocity contour.

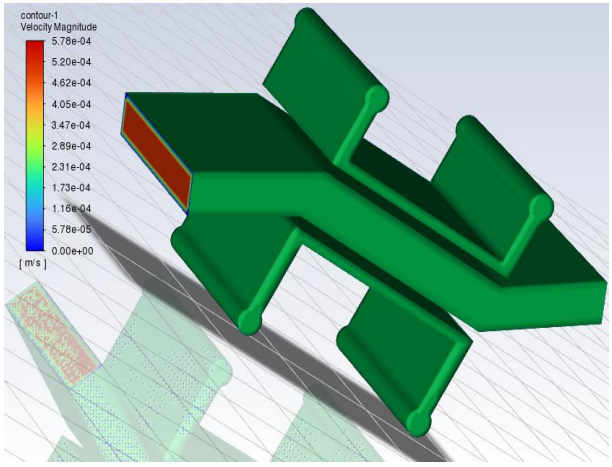


Figure 10. Velocity contour of the design

Static pressure is the pressure exerted by a fluid when it's at rest and calculated at each point within the computational domain based on the fluid properties and the flow conditions specified in the simulation. Static pressure contours reveal flow features such as areas of high and low pressure, recirculation zones, shock waves, and boundary layer behaviour. The static pressure contours are influenced by boundary conditions specified in the simulation, such as inlet velocity, outlet pressure, and wall boundary conditions. The contour plot can be customized by adjusting the contour levels. Levels define the intervals at which contour lines or color changes occur, allowing focusing on specific pressure ranges or gradients. The figure 11 shows static pressure contour.

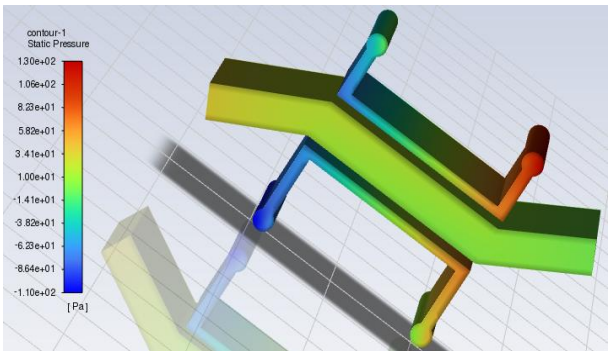


Figure 11. Static pressure contour of the design

4. EXPERIMENTAL RESULTS

The wall fluxes contour result analysis visualizes parameters like wall shear stress distribution along boundaries (Nie et al., 2007). The maximum shear stress of 3.48e+00 indicates areas with the highest stress levels, likely near high velocity or turbulent regions. Conversely, the minimum shear stress of 5.79e-03 suggests regions with lower stress, possibly near slower-moving fluid or regions of separation. The fact that the minimum value covers 90% of the inlet implies a relatively uniform stress distribution in the central area (Datta & Ghosal, 2009). As you move towards the edges, where the stress becomes maximum, it suggests regions of increased turbulence or flow disruption, common in boundary layers. The median value, 1.74e+00, likely represents the average shear stress level across the surface, indicating the typical stress experienced by the boundary. Figure 12 shows the wave flux contour analysis.

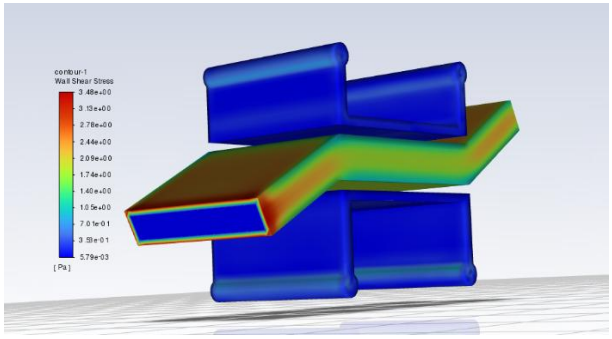


Figure 12. Wave flux contour analysis of the design

In derivatives contour analysis, the strain rate distribution is visualized across the domain. The maximum strain rate of 7.17e+02 indicates areas of intense deformation, likely concentrated around regions of high flow velocity or turbulence. Conversely, the minimum strain rate of 4.72e+02 represents areas with lower deformation or smoother flow. The observation that the near-minimum value is seen at the center of the inlet suggests that flow conditions are relatively uniform and less turbulent in this region. As we move towards

the edges, where the strain rate becomes maximum, it indicates higher levels of deformation and possibly increased turbulence, which is common in boundary layers and near walls where flow separation or recirculation may occur. Figure 13 shows the derivatives contour analysis.

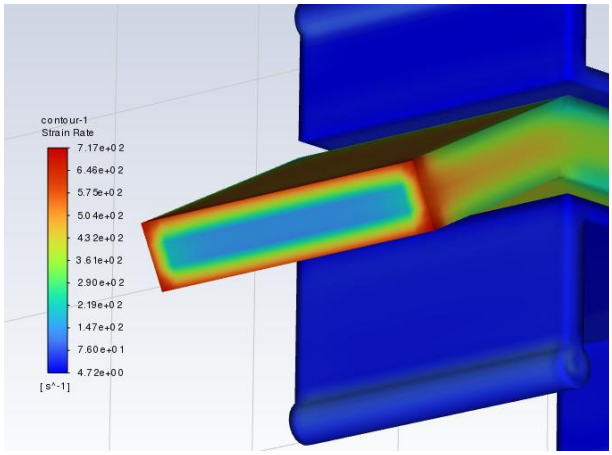


Figure 13. Derivatives contour analysis of the design

Mesh contour result analysis involves visualizing data such as mass or velocity distributions across a computational domain. In your case, the maximum mass X coordinate value being 3.00e-05 means that at a certain location (in the X direction), the highest mass value is observed. Similarly, the minimum X coordinate value of 0 indicates where the lowest mass value occurs. The median X coordinate value of 1.50e-05 signifies the middle point where half of the mass values are higher and half are lower. When analysing vertically, the upper portion of the domain displays the maximum value of the analysed parameter (mass in this case), the lower portion shows the minimum value, and the middle layer illustrates the median value. Figure 14 shows the mesh contour analysis.

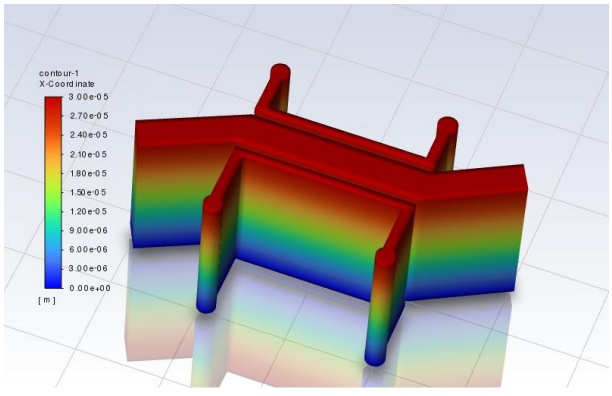


Figure 14. Mesh contour analysis of the design

Residual contour analysis is a crucial tool for evaluating the convergence of a simulation. It provides insight into how well the numerical solution is progressing towards a steady state. The reported maximum, minimum, and median mass imbalances offer a comprehensive picture of the convergence behaviour. A maximum mass imbalance of 3.39 × 10-15 indicates the highest level of numerical error encountered during the simulation, while a minimum mass imbalance of -3.18 x 10-15 signifies the lowest level of imbalance observed. The median mass imbalance of 1.05 x 10-16 serves as a reference point for the typical numerical error present in the solution. The observation that the complete middle chamber exhibits the median value suggests that convergence within this region is relatively stable and consistent. However, the slight variation observed in the two chambers, where a mixture of maximum and minimum values is present, indicates that convergence is less uniform in these areas. This variation may be due to local flow phenomena or numerical instabilities. Furthermore, the fact that the inlet displays a value close to the minimum suggests that convergence in this region is relatively good. Figure 15 shows residuals contour analysis of the design.

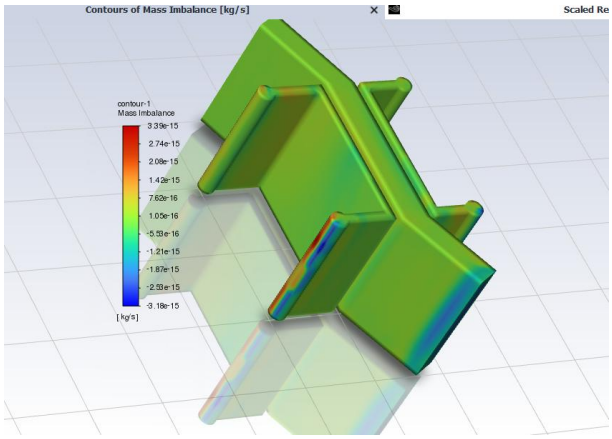


Figure 15. Residuals contour analysis of the design

The XY plot represents the results of a flow simulation, specifically focusing on the velocity magnitude at different positions within the flow domain. The black (Inlet) region exhibits a relatively constant velocity magnitude of around 5.00e-04 m/s. This suggests a uniform inflow condition. The velocity magnitude in the red (Outlet) region is higher than the inlet, fluctuating around 7.00e-04 m/s with some variations. This could indicate flow acceleration or turbulence development. Green (Wall-solid) exhibits velocity magnitude which is consistently close to 0.00e+00 m/s. This is expected as the fluid at the wall adheres to the no-slip condition, meaning it has zero velocity relative to the solid boundary. The x-axis represents the position along the flow path. The velocity magnitudes are plotted against these positions, providing insights into how the flow evolves spatially. The observed velocity profiles indicate flow through a microchannel. Flow Regime: The presence of fluctuations in the outlet region depicts the possibility of turbulent flow. The zero velocity at the wall confirms the expected behaviour of viscous fluids adhering to solid boundaries. This region is often referred to as the boundary layer, where viscous effects

are dominant. Figure 16 shows the velocity XY plot of the design.

The static pressure variation along a microchannel flow path is also represented by the XY plot. The High-Pressure Region (Inlet) is the left side of the graph exhibits a consistently high static pressure, around 70 Pa. The pressure remains relatively constant in this section, indicated by the closely clustered data points. Moving towards the right side of the graph, the static pressure drops significantly to around 0 Pa. This region is observed as a Low-Pressure Region (Outlet). Similar to the inlet, the pressure in this section remains fairly constant along the position. The transition between the high-pressure inlet and the low-pressure outlet appears to be quite abrupt. This sudden pressure drop indicates a change in flow conditions, such as a change in microchannel dimensions, the presence of a bubble, or an elevation change. Figure 17 shows static pressure XY plot of the design.

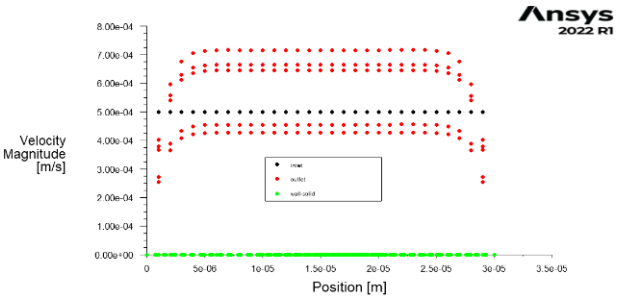


Figure 16. Velocity XY plot of the design

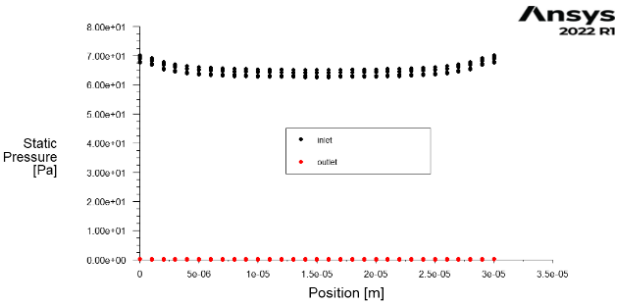


Figure 17. Static pressure XY plot of the design

5. DISCUSSION

In ANSYS Fluent, the flow rate report provides crucial insights into how fluids behave within a system. Pressure and velocity distributions demonstrate stable laminar flow regimes suitable for organ-on-chip applications (Cui & Wang, 2019). With an inlet static pressure of 6.1780928e-09 Pa (Pascal's) and an outlet pressure of 0, it indicates a scenario where the fluid enters the system with low but measurable pressure and exits into an environment where pressure is essentially negligible. The significance of the outlet pressure being 0 suggests that the fluid is not being actively propelled or pressurized as it exits the system. Instead, it's likely flowing under the influence of gravity or some other passive force. This could imply that the fluid is moving slowly, as there is no significant pressure differential to drive it with force. When the net pressure remains the same as the inlet pressure, it indicates that there are no significant pressure losses or gains within the system. This could be due to factors such as negligible friction or resistance within the flow path. Additionally, optimizing the design to minimize pressure differentials and enhance flow uniformity could improve the efficiency and effectiveness of the system (Didar & Tabrizian, 2010; Cui & Wang, 2019). Figure 18 shows the flow rate report in terms of static pressure.

Flow Rate Static Pressure	[(Pa) (kg/s)]
inlet	6.1780928e-09
outlet	0
Net	6.1780928e-09

Figure 18. Flow rate report of the design

The density report provides insights into the distribution of density within a fluid domain. When considering a solid material with a density of 1060 kg/m^3, the mass-weighted average density indicates how this density influences the overall density distribution within the domain. The net value, reflecting the solid density, signifies that the solid's density has a significant impact on the overall density, replicating it within the domain. This implies that the presence of the solid material strongly influences the density characteristics within the fluid domain, with the average density reflecting its mass-weighted contribution. Figure 19 shows density report of the design.

Mass-Weighted Average Density	[kg/m^3]
solid	1060
Net	1060

Figure 19. Density report of the design

The area report provides information about the areas of various sections in your computational domain. In your case, the inlet area is 1.8e-10 square meters, the outlet area is 1.7997486e-10 square meters, and the net area is 3.5997486e-10 square meters. This data is crucial for understanding the flow characteristics within the domain, especially in terms of mass flow rates and velocity profiles. Figure 20 shows area report of the design. Similar CFD-based evaluations have validated such microfluidic design (Gao et al., 2012).

Area	[m^2]
inlet	1.8e-10
outlet	1.7997486e-10
Net	3.5997486e-10

Figure 20. Area report of the design

6. CONCLUSION

From the analysis conducted in ANSYS Fluent with blood data imported, several key findings emerge regarding static pressure and velocity contours. The static pressure contours reveal significant variations across the design. The maximum static pressure is observed to be 1.30e+02 Pa, indicating areas of high pressure, while the minimum static pressure reaches -1.10e+02 Pa, indicating areas of low pressure. Notably, the central microchannel maintains a median static pressure of 1.00e+01 Pa. Similarly, velocity contours depict varying flow velocities throughout the design. The maximum velocity magnitude is found to be 5.78e-04 m/s, with the inlet showcasing higher velocities at its center and lower velocities at its edges. The rest of the design exhibits a median velocity of 2.89e-04 m/s. A noteworthy observation is the presence of two cyclic suction chambers, which experience the minimum static pressure, while the other two regions exhibit static pressures closer to the maximum. This suggests the presence of localized suction effects or areas of increased resistance to flow.

In conclusion, the analysis highlights the complex flow behaviour and pressure distribution within the blood flow system. Future work could focus on further investigating the dynamics within the suction chambers to understand their impact on overall flow performance.

References:

Chakraborty, S. (2005). Dynamics of capillary flow of blood into a microfluidic channel. *Lab on a Chip*, *5*(4), 421. https://doi.org/10.1039/b414566f

Chow, W. W. Y., Lei, K. F., Shi, G., Li, W. J., & Huang, Q. (2005). Microfluidic channel fabrication by PDMS-interface bonding. *Smart Materials and Structures*, *15*(1), S112–S116. https://doi.org/10.1088/0964-1726/15/1/018

Cui, P., & Wang, S. (2019). Application of microfluidic chip technology in pharmaceutical analysis: A review. *Journal of Pharmaceutical Analysis*, *9*(4), 238–247. https://doi.org/10.1016/j.jpha.2018.12.001

Datta, S., & Ghosal, S. (2009). Characterizing dispersion in microfluidic channels. *Lab on a Chip*, *9*(17), 2537. https://doi.org/10.1039/b822948c

Didar, T. F., & Tabrizian, M. (2010). Adhesion based detection, sorting and enrichment of cells in microfluidic Lab-on-Chip devices. *Lab on a Chip*, *10*(22), 3043. https://doi.org/10.1039/c0lc00130a

Gao, L. Q., Xi, Y., Fu, Q., Zhu, M. H., & Zhang, J. S. (2012). Performance analysis of a new type of wind resistance brake mechanism based on FLUENT and ANSYS. *Advanced Materials Research*, *562–564*, 1099–1102. https://doi.org/10.4028/www.scientific.net/amr.562-564.1099

Gervais, T., El-Ali, J., Günther, A., & Jensen, K. F. (2006). Flow-induced deformation of shallow microfluidic channels. *Lab on a Chip*, *6*(4), 500. https://doi.org/10.1039/b513524a

Kamholz, A. E., Weigl, B. H., Finlayson, B. A., & Yager, P. (1999). Quantitative analysis of molecular interaction in a microfluidic channel: the T-Sensor. *Analytical Chemistry*, *71*(23), 5340–5347. https://doi.org/10.1021/ac990504j

Khademhosseini, A., Suh, K. Y., Jon, S., Eng, G., Yeh, J., Chen, G., & Langer, R. (2004). A soft lithographic approach to fabricate patterned microfluidic channels. *Analytical Chemistry*, *76*(13), 3675–3681. https://doi.org/10.1021/ac035415s

Kirpo, M. (2013). Global simulation of the Czochralski silicon crystal growth in ANSYS FLUENT. *Journal of Crystal Growth*, *371*, 60–69. https://doi.org/10.1016/j.jcrysgro.2013.02.005

Mertaniemi, H., Laukkanen, A., Teirfolk, J., Ikkala, O., & Ras, R. H. A. (2012). Functionalized porous microparticles of nanofibrillated cellulose for biomimetic hierarchically structured superhydrophobic surfaces. *RSC Advances*, *2*(7), 2882-2886. https://doi.org/10.1039/c2ra00020b

Nie, F., Yamada, M., Kobayashi, J., Yamato, M., Kikuchi, A., & Okano, T. (2007). On-chip cell migration assay using microfluidic channels. *Biomaterials*, *28*(27), 4017–4022. https://doi.org/10.1016/j.biomaterials.2007.05.037

Park, S., Zhang, Y., Wang, T., & Yang, S. (2011). Continuous dielectrophoretic bacterial separation and concentration from physiological media of high conductivity. *Lab on a Chip*, *11*(17), 2893. https://doi.org/10.1039/c1lc20307j

Rybdylova, O., Qubeissi, M. A., Braun, M., Crua, C., Manin, J., Pickett, L., . . . Heikal, M. (2016). A model for droplet heating and its implementation into ANSYS Fluent. *International Communications in Heat and Mass Transfer*, *76*, 265–270. https://doi.org/10.1016/j.icheatmasstransfer.2016.05.032

Tan, Y., Fisher, J. S., Lee, A. I., Lee, A. I., Cristini, V., Lee, A. P., & Lee, A. P. (2004). Design of microfluidic channel geometries for the control of droplet volume, chemical concentration, and sorting. *Lab on a Chip*, *4*(4), 292. https://doi.org/10.1039/b403280m

Tiwari, S. K., Bhat, S., & Mahato, K. K. (2020). Design and fabrication of low-cost microfluidic channel for biomedical application. *Scientific Reports*, *10*(1), 9215. https://doi.org/10.1038/s41598-020-65995-x

Wu, J., He, Z., Chen, Q., & Lin, J. (2016). Biochemical analysis on microfluidic chips. *TrAC Trends in Analytical Chemistry*, *80*, 213–231. https://doi.org/10.1016/j.trac.2016.03.013

Xu, J., & Attinger, D. (2008). Drop on demand in a microfluidic chip. *Journal of Micromechanics and Microengineering*, *18*(6), 065020. https://doi.org/10.1088/0960-1317/18/6/065020

Yaralioglu, G. G., Wygant, I. O., Marentis, T. C., & Khuri-Yakub, B. T. (2004). Ultrasonic mixing in microfluidic channels using integrated transducers. *Analytical Chemistry*, *76*(13), 3694–3698. https://doi.org/10.1021/ac035220k

Zhou, J. Z., Xu, X. P., Chu, W. J., Zhu, Z. C., Chen, Y. H., & Lai, S. W. (2013). Analysis and Simulation of the Fluid Field in Thermal Water-Jet Nozzle Based on ANSYS FLUENT & ICEM CFD. *Applied Mechanics and Materials*, *423–426*, 1677–1684. https://doi.org/10.4028/www.scientific.net/amm.423-426.1677

Manasi Mahajan
Vellore Institute of Technology
Chennai
India
mahajan.manasi2023@vitstudent.ac.in
ORCID 0009-0005-7490-1404

Manisha R.
Vellore Institute of Technology
Chennai
India
manisha.r2022@vitstudent.ac.in
ORCID 0009-0003-0100-0627

Reena Monica P.
Vellore Institute of Technology
Chennai
India
reenamonica@vit.ac.in
ORCID 0000-0002-8202-4027